RSC Advances

ROYAL SOCIETY OF CHEMISTRY

www.rsc.org/advances

Growth of carbon composites by grafting on pregrown vertically aligned single-walled carbon nanotube arrays and their use in high power supercapacitors

Xiujun Fan[†‡⊥], Haiqing Zhou[‡⊥], Xia Guo[†]*

[†]*College of Electronic Information and Control Engineering, Beijing University of Technology, Beijing 100124, China*

[‡]*Department of Chemistry, [⊥]Richard E. Smalley Institute for Nanoscale Science and Technology, Rice University, Houston, Texas 77005, United States*

Corresponding Author

fxiujun@gmail.com (X. J. Fan)

Carbon composite materials consisting of onion-like carbons (OLCs) and vertically aligned graphene nanoribbons (VA-GNRs) has been efficiently prepared by atomic hydrogen treatment. SiC is employed as the seed for growing nanodiamonds, which are served as precursors and converse into OLCs. The obtained OLCs are quasi-spherical shaped with closed concentric graphite shells without core. The original vertical structural integrity and alignment of VA-GNRs is well preserved, and the OLCs remains highly porous. The electrochemical measurements show that the OLC-GNRs composite exhibit higher capacitive properties than original vertically aligned single walled carbon nanotubes (VA-SWCNTs) carpet and VA-GNRs. This composite nanostructure demonstrates high performance in maximum specific energy (36.4 Wh kg^{-1}), specific power (270.2 kW kg^{-1}), and cycle stability (no drop after 10,000 cycles). The superior electrochemical performance of the OLCs-GNRs composite electrode can be attributed to higher specific surface area of the additional porous OLCs, and the vertical

alignment of the conductive paths of VA-GNRs. All demonstrate that atomic hydrogen treatment is an attractive approach to fabricate electrodes for supercapacitors with high power and energy density.

Introduction

Owing to the capability of providing instantaneously a higher power density than batteries and higher energy density than conventional dielectric capacitors, supercapacitors or electrochemical capacitors have attracted vast attention and been widely used in portable electronics, power back-up, electrical vehicles and various microdevices[1]. However, the low energy density of supercapacitors (usually less than 10 Wh kg^{-1}) greatly limits their further application[2]. Therefore, the improvement of energy density of supercapacitors without sacrificing their high power capability to be close to or even beyond that of batteries remains a big challenge. Consequently, carboneous materials, such as carbon nanotubes (CNTs)[3, 4], graphene nanosheets[5] and conducting polymers[6], transition-metal oxides[7, 8], and composites[2, 9] have been used to fabricate high energy density supercapacitor electrodes. Among these candidated electrode materials, onion-like carbons (OLCs) with concentric shells of graphitic carbon, interior void space, spherical shape and nanosize, possessing high specific surface area, and high chemical stability have been considered as an ideal candidate for the applications in the renewable energy storage and power output technologies, especially high energy density supercapacitors[10].

Numerous methods currently exist to produce OLCs, including electron irradiation[11, 12], ion implantation[13], plasma-enhanced chemical vapor deposition (CVD)[14, 15], thermal treatment of nanodiamonds[16, 17], and arc discharge of carbon electrode[18]. Among those, OLCs synthesized from nanodiamonds powders have attracted significant attention because of their superb properties including (i) high BET surface area (500 m^2/g), (ii) high electrical conductivity, (iii) high thermal stability, (iv) appropriate mesoporous structure, and (v) high quality, high yield[19]. Recently, Shinji Hayashi *et al* [20, 21] prepared carbon onions in large quantities by annealing ultra-disperse diamond (UDD) powder (2-6 nm) at ~ 1700 ℃ whereupon UDD was transformed into OLCs from the surface of the particle proceeding

inward to the center. Though this method is high yield, it requires very high temperatures and high pressures to convert the diamond cluster into OLCs. In additional, some preparation techniques like ball milling[22] and shock-compressing[23] have been developed to obtain nanoscale OLCs. Unfortunately, they are generally remain more or less the following disadvantage: high cost, large sphere dimensions and poor graphitic crystallinity with many byproducts. In this context, it is still challenging but desirable to develop an efficient way to synthesize OLCs with high crystallinity.

Meanwhile, graphene nanoribbons (GNRs) being CNTs that have been unzipped longitudinally into ribbons are considered potential candidates for energy storage electrodes[24], due to their high specific surface area (SSA), excellent electrical conductivity, and chemical stability[25]. For carbon materials, their SSA and porosity are essential to their electrochemical performance in supercapacitors. From this point of view, the vertically aligned graphene ribbons (VA-GNRs) array appears to be advantageous over randomly deposited GNRs powder in which aggregation of active materials would compromise the porosity and available SSA. Combination of VA-GNRs and OLCs, while maintaining the vertically integrity of the VA-GNRs and porous nature of OLCs should further increase the accessible surface area, thus facilitating various device fabrications. However, experimental fabrication of this material is challengeable and report about OLCs-GNRs composite is rare. Herein, we report a simple method to synthesize OLCs from nanodiamonds seeded with SiC, and prepare composite nanoscale materials composed of OLCs and VA-GNRs (OLCs-GNRs). By analyzing the evolutions in morphology and structure, we propose a model to elucidate the growth mechanism of OLCs from nanodiamonds. The supercapacitor built from the OLCs-GNRs composite electrodes offered an extremely small equivalent series resistance (ESR), thus obtained a high power and energy density (270.2 kW kg^{-1}, 36.4 Wh kg^{-1}); and also exhibited superior frequency response.

Results and discussion

Fig. 1a is an illustration of the process for preparing OLCs and VA-GNRs (OLCs-GNRs), in which a thin layer of Si nanoparticle was deposited on vertically aligned single walled carbon nanotubes (VA-SWCNTs) with an e-beam evaporator[26] (for more details, see the experimental section). Next, atomic hydrogen treatment on the samples was carried out using a mixture of H_2 (140 sccm), H_2O (15 sccm) and CH_4 (0.75 sccm) at 25 Torr and 850 °C for 2-6 h. During this process, the Si nanoparticles reacted with carbon source (CH_4) and formed SiC, which provided sites and seeds for nanodiamonds nucleation and growth. And then, the sp^3-bonded nanodiamonds were gradually transformed into sp^2 carbon nanospheres (**Fig. S1c**), simultaneously atomic hydrogen introduced unzipping VA-SWCNTs (VA-GNRs) (**Fig. S1b**), thus the composite material consisting of OLCs and VA-GNRs was obtained (**Fig. S1d**). As revealed in **Fig. 1b**, the pristine VA-SWCNT carpet features high density and vertically aligned, and individual nanotubes densely packed and uniformly distributed throughout the whole substrate. As shown in **Fig. S2** and **S3**, atomic hydrogen treated VA-SWCNTs possess rough surface with some small particles. Raman spectrum show that the I_G/I_D ratios increased with increasing of treated time, which is due to the atomic hydrogen etching effect[27]. VA-SWCNTs treated at 850 °C for 6 h are referred as OLCs-GNRs, and this designation is used here-after. **Fig. 1c** is a low-magnification SEM image of OLCs-GNRs, revealing a layer of OLCs network capping on the composite. The thickness of the OLCs network is approximately 5-10 μm (**Fig. 1d**). The OLCs-GNRs composite arrays are quite aligned, and cannot easily be peeled off from the substrate without destroying the integrity due to the carbon network on top of the composite (**Fig. 1c** inset). After atomic hydrogen treatment, as shown in **Fig. 1e** and **S4**, the resultant nanotubes become flattened with opening walls and the widths are widened due to the transformation from VA-SWCNTs to unzipped CNTs (VA-GNRs). The aligned pores of VA-GNRs together with mesopores of OLCs (**Fig. 1c** inset) could be beneficial for the introduction and transport of electrolyte ions when compared to the pristine VA-SWCNTs. The average I_G/I_D ratio of the OLCs-GNRs is lower than that of the VA-SWCNTs treated for 2 and 4 h (**Fig. 1f, S2c** and **S3c**), which can be attributed to the increased number of carbon defects introduced by the atomic hydrogen reaction [28]. The intensity of the 2D-band are 80-100% as that of the G band, and along with the D-band shows a small shoulder (D' peak, black arrow), due to the formation of a few layers of

graphene ribbons[29], which is consistent with the result of TEM images (**Fig. 1e**, and **S4**). These findings suggest that atomic hydrogen treatment can unzip VA-SWCNTs with low defect. An OLCs-GNRs composite film transferring from the substrate is shown in **Fig. 1g**. After acid-etching and transferring, the structure of the composite film can be preserved without any collapse[30].
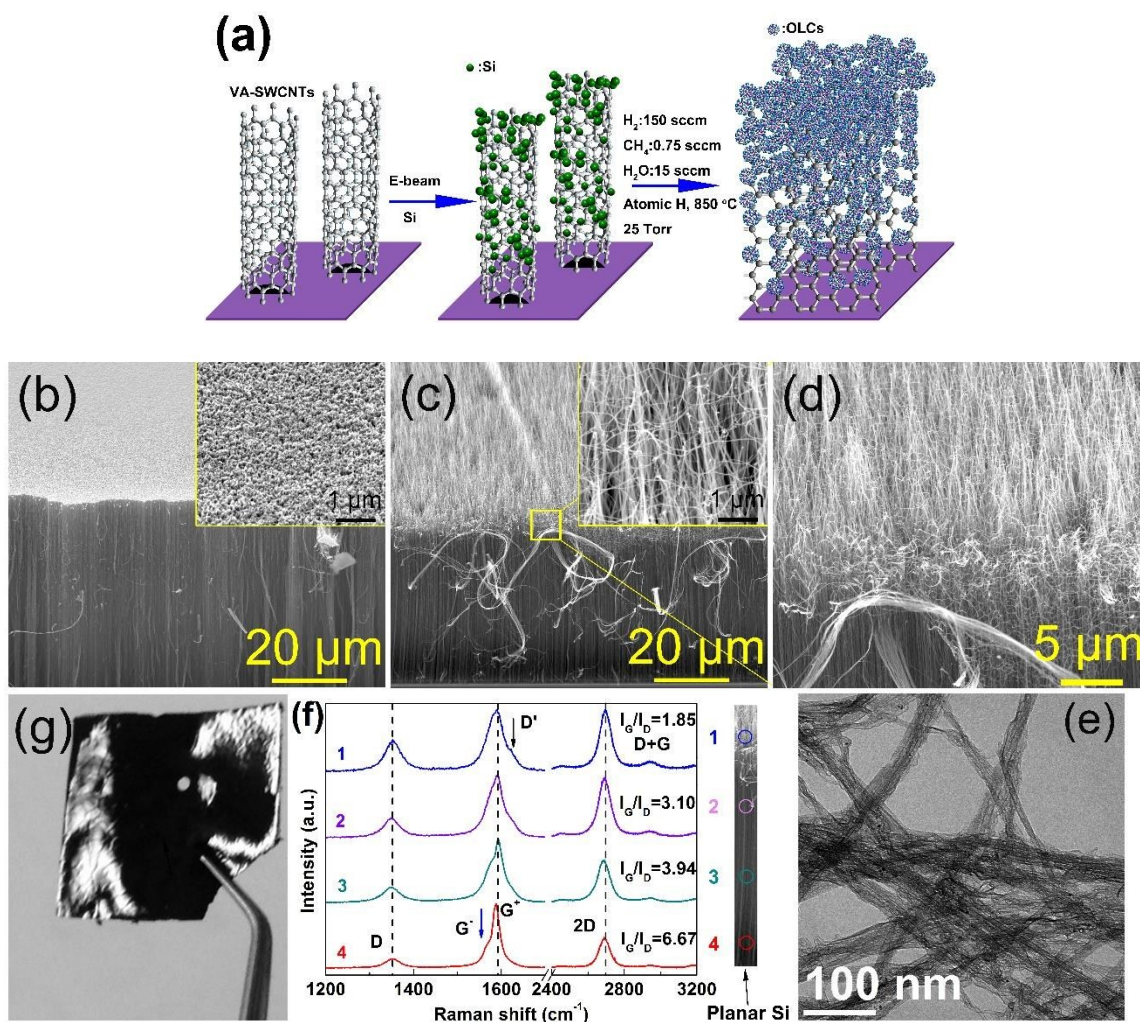

Fig. 1. (a) Scheme illustration of the formation of composite material of OLCs-GNRs. SEM images of (b) the pristine VA-SWCNTs carpet and (c-d) for OLCs-GNRs, respectively. (e) TEM image of GNRs. (f) Raman spectroscopy and OLCs-GNRs, colored circles indicate locations where the Raman spectra were collected. The diameter of the colored dots represents 2 μm. (g) Photograph of an OLCs-GNRs composite film transferred from the Si substrate.
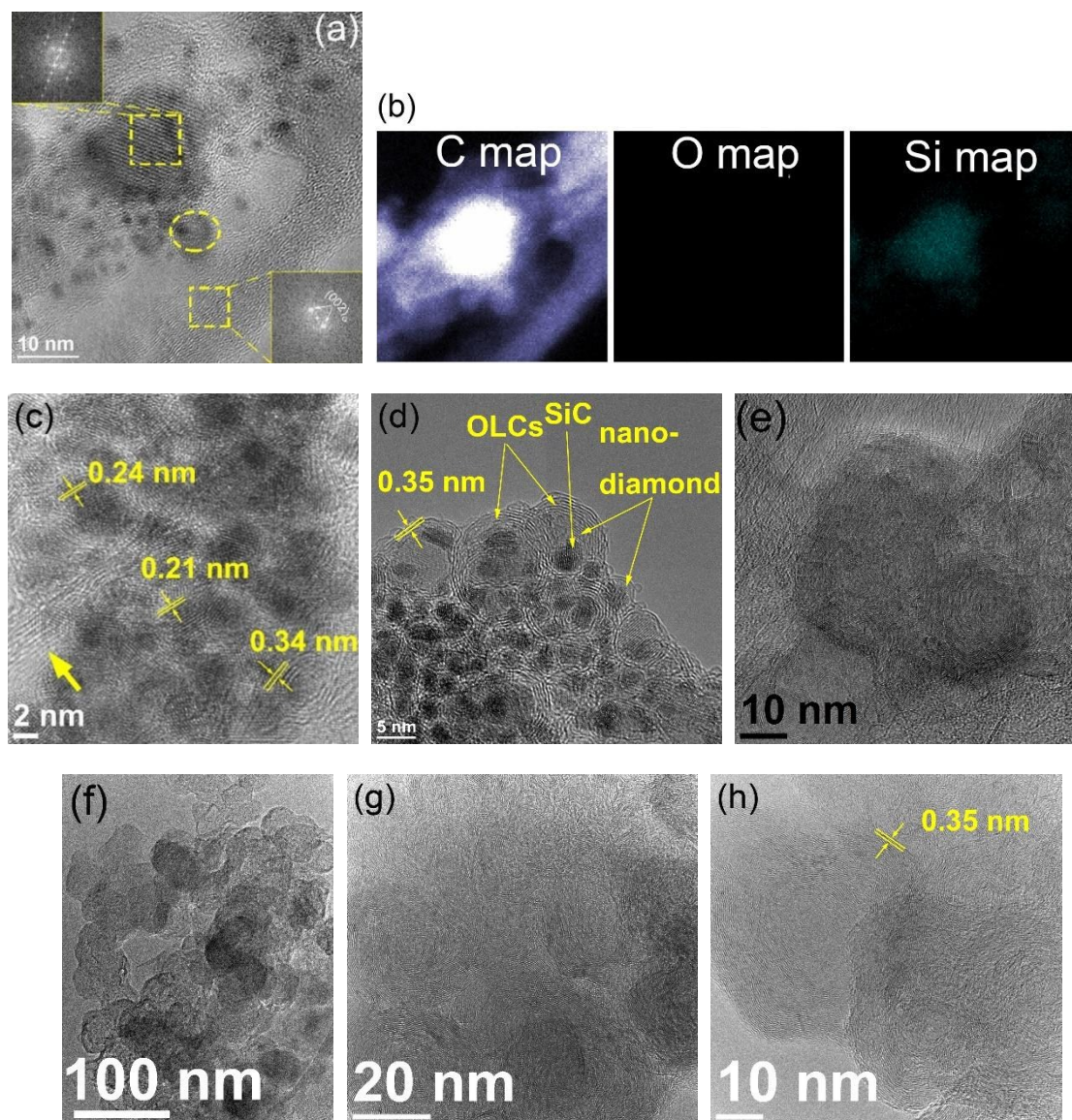
Fig. 2. (a) TEM images of the unzipped carbon nanotube, SiC and nanodiamonds clusters grown at 850 °C for 2 h and (b) the corresponding EDS mapping images of C, O and Si. (c-d) TEM image of nanodiamonds and SiC clusters from the OLCs-GNRs grown at 850 °C for 2 h, (e) for 4 h. (f-h) TEM images confirm that nanodiamonds have been converted to OLCs grown at 850 °C for 6 h, (h) the OLCs reveal multi-layered structures.

Fig. 2a and S5 illustrates transmission electron microscope (TEM) images of VA-SWCNTs carpets with 3 nm silicon treated with atomic hydrogen at 850 ℃ for 2 h. The fast-Fourier Transform (FFT)

pattern presented in the left inset of **Fig. 2a** indicates SiC nanoparticles, and the right inset indicates the

(002) crystallographic graphite layer separated by 0.35 nm. The smaller, ~ 1 nm diameter SiC particles

have a round-shape groove on the bottom coated with diamond that is a nucleation site[31], whereas the

larger SiC nanoparticles should arise from the agglomeration of smaller ones. Energy-dispersive

spectrometry (EDS) measurements reveal that the SiC and nanodiamond cluster contained only C, Si

and O, and the Si atoms being highly concentrated at the nanoparticles with very few O atoms (**Fig. 2b**).

Fig. 2c indicates that some silicon particles have reacted with carbon and transformed into SiC

(d_{111}=0.24 nm) and nanodiamond clusters (d_{111}=0.21 nm) with atomic hydrogen treatment for 2 h.

Additionally, some straight unzipped carbon nanotubes with lattice spacing of ~ 3.4 Å are observed,

suggesting the CNTs have been transformed into graphene ribbons (right corner in **Fig. 2a**, indicated by

yellow arrow in **Fig. 2c**, and **Fig. S5**). **Fig. 2d** shows the surfaces of SiC and nanodiamond cluster

consist of two to six sp^2 graphitic shells with diameters ranging from 5 to 20 nm. As the atomic

hydrogen treatment time prolonged to 4 h, the SiC nanoparticles are totally vanished and nanodiamonds

have been transformed into sp^2 graphitic shells (**Fig. 2e**, and **S6**). The obtained OLCs nanoparticles

without core are obvious larger than the size of SiC or nanodiamond particles in **Fig. 2c** and **d**. With

atomic hydrogen treatment for 6 h, most OLCs particles with multi-layered structures smaller than 50

nm are observed (**Fig. 2f**). Carbon onions, carbon encapsulated nano-onions without cores or holes at

the center are also present in AFM images (**Fig. S7**). **Fig. 2g** demonstrates a HR-TEM image where the

majority of nanodiamond particles have been converted into quasi-spherical particles with diameters

between 20-50 nm and closed concentric shells. OLCs particles are 50 nm in diameter with ordered

concentric shells are formed (**Fig. 2h**). The distance between the shells is approximately 0.35 nm which

closely matches the lattice parameter ($d_{002} = 0.34$ nm) of bulk graphite. These observations reveal that

atomic hydrogen treatment effectively transform diamond particles/clusters into OLCs, while

nanodiamonds are used as precursors, and SiC nanocrystals are the seeds for nanodiamonds nucleation

and growth[31]. In order to compare the supercapacitor performance of OLCs-GNRs with that of GNRs,

the VA-GNRs were obtained with the same treatment condition as OLCs-GNRs (**Fig. S8**). OLCs

particles become larger than the nanodiamond precursor and demonstrate an increasing degree of

structural order with prolonging treatment time. This is because of the lower density of graphitic carbon[32]. In addition, the combination of the porous structure dramatically increased the surface area: N_2 sorption-desorption measurements give SSA of 105, 278 and 752 m^2/g for VA-SWCNTs, VA-GNRs and OLCs-GNRs, respectively (**Table S1**). The additional surface area in the OLCs-GNRs composite structure enhances the electrochemical properties of a supercapacitor by providing a large area for the electrolyte ions to interact with the electrode surface[33].
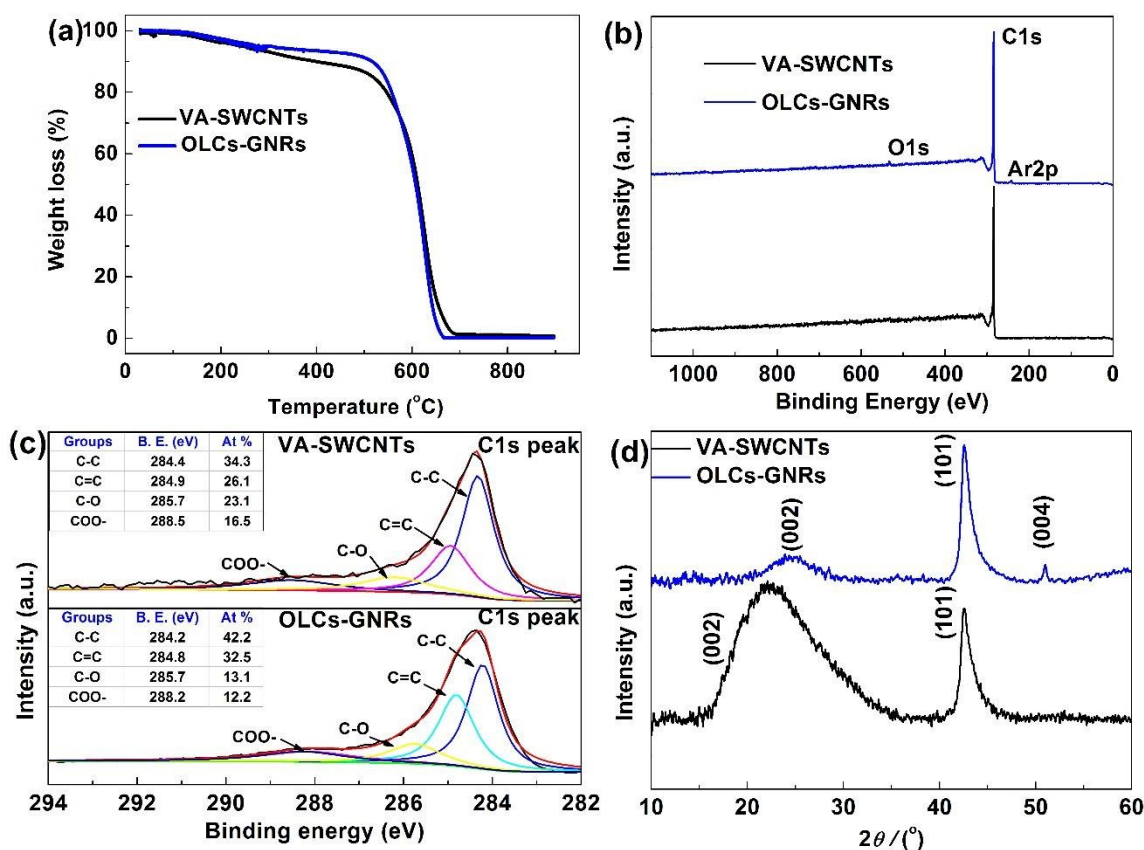

Fig. 3. (a) TGA curves of the VA-SWCNTs carpet (black curve) and OLCs-GNRs (green curve) measured by heating samples in air flow to 900 ℃ at a heating rate of 5 ℃ min^{-1}. XPS spectra (b-c) and XRD pattern (d) of the VA-SWCNTs carpets and OLCs-GNRs.

Next, thermogravimetric analysis (TGA) was carried out for the as-prepared VA-SWCNTs and OLCs-GNRs. The weight loss for VA-SWCNTs and OLCs-GNRs both start to occur at ~ 490 ℃ and continue to increase rapidly during TGA analysis, which is the typical temperature behavior of high quality

carbon materials[34]. The OLCs-GNRs has an oxidation temperature ~ 675 ℃, exhibiting only one exothermal event. The overall thermal stability is very good and residual mass is small, which provides additional evidence that the obtained GNRs are neither damaged nor derivatized with the atomic hydrogen treatment process. The structural changes of VA-SWCNTs with atomic hydrogen treatment were further characterized with X-ray photoelectron spectroscopy (XPS) spectra and diffraction (XRD) pattern. As displayed in **Fig. 3b**, the slight increase in oxygen signal after atomic hydrogen treatment can be attributed to physisorbed oxygen, which can be further confirmed by high-resolution O 1s XPS spectra of VA-SWCNTs and OLCs-GNRs in **Fig. S9. Fig. 3c** exhibits the C1s high resolution spectra of the pristine VA-SWCNTs and OLCs-GNRs. The C/O ratio increases from 49.7% to 74.7%, the C-C and C=C peaks shape become broader, and sp^2 C-C bond increases slightly from 34.3% up to 42.2%, demonstrating that some amorphous-like carbon was removed and the produced nanoribbons are crystalline[35], which is consistent with Raman spectrum (**Fig. 1f**). The increased C/O ratio also indicates that litter edge oxidation process (oxygenated groups adsorbed on the surface) occurring during atomic hydrogen treatment[35]. And the increased sp^3 C=C band can be attributed to the nanodiamond drived carbon onion. The XRD patterns of VA-SWCNTs and OLCs-GNRs are shown in **Fig. 3d**. The diffraction main peaks at 22.3 °and 42.6 °observed in the diffraction of VA-SWCNTs can be attributed to the hexagonal graphite structures (002), and (101) (PDF # 00-050-0926). For the OLCs-GNRs, peak (002) becomes narrow and shifts slightly to higher 2θ, and peak (004) together with a sharp (101) peak is observed, implying that atomic hydrogen treatment can get rid of graphitic carbon impurities[28], which is consistent with the results of Raman spectrum and TGA curve. The OLCs-GNRs are in graphite form, with large regions of crystallinity[36]. SiC and Si compounds peak are so weak that can't be detected. Therefore, SEM, XRD, TEM and XPS demonstrate high quality OLCs-GNRs prepared with HF-CVD process, which is desired for high-performance supercapacitor.
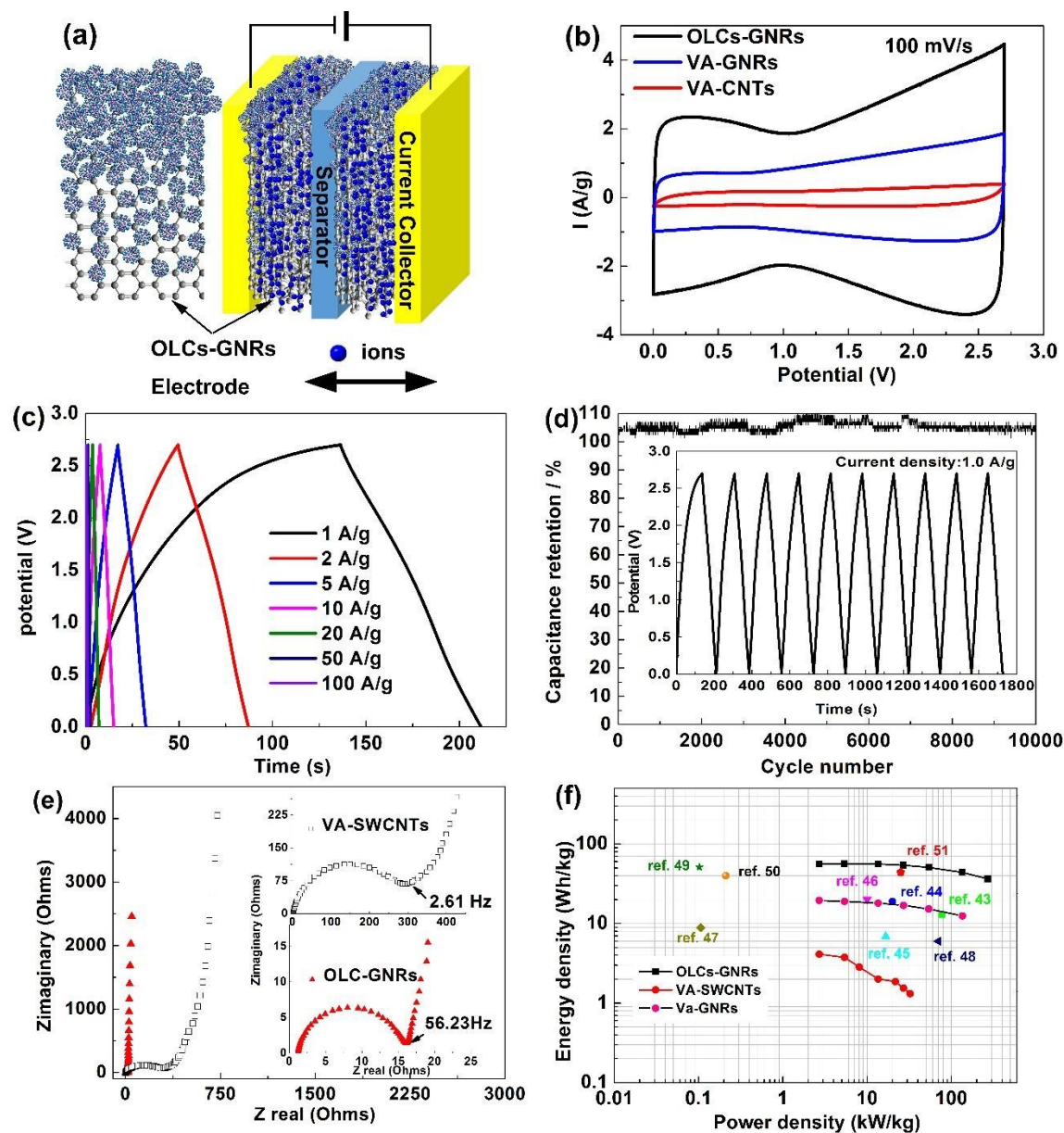
Fig. 4. (a) Scheme of supercapacitor fabrication. (b) CVs of supercapacitors the VA-SWCNTs carpets, VA-GNRs and OLCs-GNRs obtained at a scan rate of 100 mV s^{-1}. (c) Galvanostatic charge-discharge curves of the device under different current densities. (d) The long-term cycling stability and Galvanostatic charge-discharge curves of the device under constant current densities (1.0 A/g). (e) Complex-plane impedance spectrum of the supercapacitor made of the VA-SWCNTs carpets and OLCs-GNRs composite. (f) Ragone plot of the VA-SWCNTs carpets, VA-GNRs and the OLCs-GNRs composite in this work compared to previous studies.

A schematic of the fabricated supercapacitor from the composite OLCs-GNRs material is illustrated in

(**Fig. 4a**). The supercapacitor device composes of stainless steel plates as current collectors (yellow),

OLCs-GNRs composite as the electrode materials and a piece of filter paper as separator (blue). 1 M

Tetraethyl Ammonium Tetrafluoroborate (TEABF$_4$) solution is filled into the system as the electrolyte

for the ion diffusion. Electrolyte ions are represented by the green dots. CVs were recorded at scan rates

from 0.1 to 100 V s^{-1} in the potential range between 0 - 2.7 V to test the power capability of the

microsystem. As seen in **Fig. 4b**, the OLCs-GNRs composite-based supercapacitor exhibits greatly

enhanced electrochemical performance compared to that of the pristine VA-SWCNTs and VA-GNRs.

The highest capacitance is ca. 104.6 F/g obtained in the OLCs-GNRs at a scan rate of 100 mV/s, in

contrast to 21.2 F/g for VA-GNRs, 8.3 F/g for VA-SWCNTs, respectively. Thought this result is lower

than that some carbon support metal oxide[37], is higher than other pure carbon hybrid materials such as

the G/SWCNT hybrids[38]. The CVs at scan rates from 50 to 1,000 mV s^{-1} exhibit almost mirror images

with respect to the zero-current line (**Fig. S10a**). The CV curves reveal a rapid current response on

voltage reversal at each end potential, presenting a quite rectangular shape, which is a clear proof of

well-enhanced capacitance properties. Moreover, the straight rectangular sides indicate that there are

negligible internal, interfacial and contact resistances[39]. In contrast, a large resistance will distort the

response, resulting in a narrower loop with an oblique shape, especially at a high scan rate[30]. **Fig. S10b**

displays a linear dependence of the average current on the scan rate up to at least 100 V s^{-1}, indicating

high performance capacitor devices[40].

Galvanostatic charge-discharge (GCD) and electrochemical impedance spectroscopy (EIS)

measurements were carried to further evaluate the electrochemical performances of the device. **Fig. 4c**

shows typical charge-discharge curves of OLCs-GNRs at different current densities. Good linear

potential-time profiles were achieved, demonstrating a good capacitance performance of the devices.

The symmetrical triangle curves indicate good reversibility of the OLCs-GNRs electrode. Additionally,

negligible voltage drop (*IR* drop) can be seen from the curve, indicating a really low internal resistance.

It is noted that as the electrode weight increased to ~ 1.0 mg, the capacitance decreased from 104.6 to 99.5 F g^{-1} at a scan rate of 100 mV/s with an increased R_s of 2.2 Ω (**Fig. S11**), which in turn lowers the energy density and power density values to ∼53.6 Wh kg^{-1} and 2.7 kW kg^{-1}, respectively. Further, cyclic stability test on the OLCs-GNRs composite electrode based supercapacitor affords stable capacitance up to 10,000 charge/discharge cycles with almost no decay (**Fig. 4d**). A typical constant current charge/discharge (E-t) curve for the OLCs-GNRs electrode is displayed inset in **Fig. 4d**. The E-t responses of the charge process reveal almost the mirror image of their corresponding discharge counterparts, and no *IR* drop is observed, demonstrating excellent electrochemical stability of OLCs-GNRs.

More importantly, supercapacitor built on the OLCs-GNRs composite electrodes also displayed superior frequency response. **Fig. 4e** reveals a complex-plane plot of the impedance of the supercapacitor. The impedance curve intersects the real axis at a 45 º angle, reflects that OLCs-GNRs has a porous structure as confirmed by SEM images[41]. Note that the 'knee' frequency in the impedance plot shown in **Fig. 4e** is about 56.23 Hz, which is about 20 and 3 times of the pristine VA-SWCNTs and VA-GNRs (**Fig. S12c**), suggesting that most of its stored energy is accessible at frequencies as high as 56 Hz. Since a better frequency response means a better power performance. This great improvement in frequency response of OLCs-GNRs composite materials constitutes a substantial advance in the rate of charge and discharge of the supercapacitor. From **Fig. 4e** and **S12c**, it can be seen that the R_s values are 5.6, 3.4 and 1.0 Ω for symmetric cells based on the pristine VA-SWCNTs, VA-GNRs and the OLCs-GNRs composite, respectively. The R_s includes intrinsic resistance of electrode materials, ionic resistance of electrolyte and contact resistance between electrode and current collector. The OLCs-GNRs composite is characterized as porous structures with significant volume of mesopores, thus enabling the excellent electrolyte access to the porous network in the composite. In addition, the GNRs in the composites form a highly conductive network, thus reduce the internal resistance within the composite electrode itself. It should be noticed that, with wet etching process, the composite is detached from the Si wafer, and get rid of the catalyst particles, forming free-standing OLCs-GNRs composite film[30] (**Fig. 1g**). This free

standing film provides a direct conductive path between the thin film electrode and the current collector; therefore the contact resistance is also significantly reduced. The charge transfer resistance (R_{ct}) caused by Faradic reactions and EDLC (C_{dl}) at the electrode/electrolyte interface, also decreases from 309.6 to 15 Ω after OLCs growth (Supporting Information, **Table S1**). The degradation of the R_s and R_{ct} values is due to the feature structure of the OLCs-GNRs composite structure. The reduced R_s is directly related to an efficient power density. From the physics aspect, the superior frequency response of OLCs-GNRs is due to small ESR[42] and the excellent electrolyte access to the thin composite through its unique porous network formed with atomic hydrogen treatment.

Fig. 4f is the Rogone plot, showing the energy density with respect to the average power density of the OLCs-GNRs composite. The energy density and power density are in the range of 36.4-56.4 Wh/kg and 2.7-270.2 kW/kg, respectively, indicating that ultrafast ion and electron transport is taking place. The OLCs-GNRs composite affords a power density up to 270.2 kW/kg, while maintaining an energy density of ∼ 36.4 Wh/kg. These values are higher than other carbon based asymmetric supercapacitor reported previously[43-51]. As a comparison, maximum energy densities of ∼ 4.1 and 19.48 Wh/kg are obtained for the pristine VA-SWCNT and VA-GNRs, respectively. And the maximum power densities are ∼32.4 and 135 kW/kg at energy densities of 1.32 and 12.48 Wh/kg for VA-SWCNTs and VA-GNRs, respectively. The OLCs have been demonstrated to be potent conductive additives to enable fast charge/discharge rates[39], thus improve the power handling ability and reduce ESR of supercapacitor electrodes. The significant improvement of the electrochemical performance of OLCs-GNRs composite is mainly attributed to: 1) the interconnection of GNRs with OLCs can form a conductive network for the transport of electrons, thus reduce the internal resistance of the electrode, leading to the high power/energy performance; 2) the introduction of OLCs can provide diffusion path on the surface of GNRs, facilitating the electrolyte ions' diffusion and migration in the electrode during rapid charge/discharge processes; 3) the wide cell voltage of 2.7 V[51, 52].

Conclusions

Carbon composite of OLCs-GNRs which preserved of vertical structural integrity of VA-GNRs and mesoporous nature OLCs have been realized by atomic hydrogen treatment. SiC seeded nanodiamonds are served as precursors and converse into OLCs, which are quasi-spherical shaped with closed concentric graphite shells without core. The supercapacitors built on the OLCs-GNRs composite electrode exhibit nearly ideal cyclic voltammograms, achieve a relative high specific capacitance of 104.6 F g^{-1} at scan rate of 100 mV/s, with a power density of 270.2 kW kg^{-1} and an ultrahigh energy density of 36.4 Wh kg^{-1}. The OLCs-GNRs composite electrode also exhibit stable cycle stability and AC frequency response. The superior electrochemical supercapacitor performance of the OLCs-GNRs composite electrode originates from high SSA due to the additional porous OLCs, and the vertical alignment of the conductive paths between the GNRs. This composite materials preparation technique has the advantages that no catalyst is required, and it is simple and fast. All demonstrate that atomic hydrogen treatment is an attractive approach to fabricate electrodes for supercapacitors with high power and energy density.

Acknowledgment

Notes and references

1. Yan, J.; Fan, Z.; Sun, W.; Ning, G.; Wei, T.; Zhang, Q.; Zhang, R.; Zhi, L.; Wei, F. *Adv. Funct. Mater.* **2012,** 22, (12), 2632-2641.

2. Long, C.; Wei, T.; Yan, J.; Jiang, L.; Fan, Z. *ACS Nano* **2013,** 7, (12), 11325-11332.

3.   Liu, J.; Zhang, L.; Wu, H. B.; Lin, J.; Shen, Z.; Lou, X. W. *Energy Environ. Sci.* **2014,** 7, (11), 3709-3719.

4.   Izadi-Najafabadi, A.; Yamada, T.; Futaba, D. N.; Yudasaka, M.; Takagi, H.; Hatori, H.; Iijima, S.; Hata, K. *ACS nano* **2011,** 5, (2), 811-819.

5.   Yoon, Y.; Lee, K.; Kwon, S.; Seo, S.; Yoo, H.; Kim, S.; Shin, Y.; Park, Y.; Kim, D.; Choi, J.-Y.; Lee, H. *ACS Nano* **2014,** 8, (5), 4580-4590.

6.   Zhao, Y.; Liu, B.; Pan, L.; Yu, G. *Energy Environ. Sci.* **2013,** 6, (10), 2856-2870.

7.   Higgins, T. M.; McAteer, D.; Coelho, J. C. M.; Sanchez, B. M.; Gholamvand, Z.; Moriarty, G.; McEvoy, N.; Berner, N. C.; Duesberg, G. S.; Nicolosi, V.; Coleman, J. N. *ACS Nano* **2014,** 8, (9), 9567-9579.

8.   Ye, J. S.; Cui, H. F.; Liu, X.; Lim, T. M.; Zhang, W. D.; Sheu, F. S. *Small* **2005,** 1, (5), 560-565.

9.   Jung, N.; Kwon, S.; Lee, D.; Yoon, D.-M.; Park, Y. M.; Benayad, A.; Choi, J.-Y.; Park, J. S. *Adv. Mater.* **2013,** 25, (47), 6854-6858.

10. Liu, Y.; Kim, D. Y. *Electrochim. Acta* **2014,** 139, (0), 82-87.

11. Banhart, F. *J. Appl. Phys.* **1997,** 81, (8), 3440-3445.

12. Roddatis, V.; Kuznetsov, V.; Butenko, Y. V.; Su, D.; Schlögl, R. *Phys. Chem. Chem. Phys.* **2002,** 4, (10), 1964-1967.

13. Cabioc'h, T.; Jaouen, M.; Denanot, M.; Bechet, P. *Appl. Phys. Lett.* **1998,** 73, (21), 3096-3098.

14. Cheng, H.-F.; Horng, C.-C.; Chiang, H.-Y.; Chen, H.-C.; Lin, I. N. *J. Phys. Chem. C* **2011,** 115, (28), 13894-13900.

15. Tzeng, Y.; Chen, W. L.; Wu, C.; Lo, J.-Y.; Li, C.-Y. *Carbon* **2013,** 53, (0), 120-129.

16. Portet, C.; Yushin, G.; Gogotsi, Y. *Carbon* **2007,** 45, (13), 2511-2518.

17. Osswald, S.; Yushin, G.; Mochalin, V.; Kucheyev, S. O.; Gogotsi, Y. *J. Am. Chem. Soc.* **2006,** 128, (35), 11635-11642.

18. Koskinen, J.; Anttila, A.; Hirvonen, J.-P. *Surf. Coat. Technol.* **1991,** 47, (1), 180-187.

19. Costa, G. C. C.; Shenderova, O.; Mochalin, V.; Gogotsi, Y.; Navrotsky, A. *Carbon* **2014,** 80, (0), 544-550.

20. Tomita, S.; Fujii, M.; Hayashi, S. *Phys. Rev. B* **2002,** 66, (24), 245424.

21. Tomita, S.; Burian, A.; Dore, J. C.; LeBolloch, D.; Fujii, M.; Hayashi, S. *Carbon* **2002,** 40, (9), 1469-1474.

22. Lee, J. Y.; Cho, K. H.; Lim, D. P.; Lee, Y. B.; Lim, D. S. *Appl. Phys. A* **2007,** 88, (4), 693-697.

23. Niwase, K.; Homae, T.; Nakamura, K. G.; Kondo, K. *Chem. Phys. Lett.* **2002,** 362, (1–2), 47-50.

24. Kosynkin, D. V.; Higginbotham, A. L.; Sinitskii, A.; Lomeda, J. R.; Dimiev, A.; Price, B. K.; Tour, J. M. *Nature* **2009,** 458, (7240), 872-876.

25. Kosynkin, D. V.; Lu, W.; Sinitskii, A.; Pera, G.; Sun, Z.; Tour, J. M. *ACS Nano* **2011,** 5, (2), 968-974.

26. Amama, P. B.; Pint, C. L.; Kim, S. M.; McJilton, L.; Eyink, K. G.; Stach, E. A.; Hauge, R. H.; Maruyama, B. *ACS nano* **2010,** 4, (2), 895-904.

27. Xiujun Fan, Z. P., Yang Yang, Haiqing Zhou, Xia Guo. *unpublished results*.

28. Talyzin, A. V.; Luzan, S.; Anoshkin, I. V.; Nasibulin, A. G.; Jiang, H.; Kauppinen, E. I.; Mikoushkin, V. M.; Shnitov, V. V.; Marchenko, D. E.; Noréus, D. *ACS nano* **2011,** 5, (6), 5132-5140.

29. Talyzin, A. V.; Luzan, S.; Anoshkin, I. V.; Nasibulin, A. G.; Jiang, H.; Kauppinen, E. I.; Mikoushkin, V. M.; Shnitov, V. V.; Marchenko, D. E.; Noréus, D. *ACS nano* **2011,** 5, (6), 5132-5140.

30. Zhang, C.; Peng, Z.; Lin, J.; Zhu, Y.; Ruan, G.; Hwang, C.-C.; Lu, W.; Hauge, R. H.; Tour, J. M. *ACS nano* **2013,** 7, (6), 5151-5159.

31. Lee, S. T.; Peng, H. Y.; Zhou, X. T.; Wang, N.; Lee, C. S.; Bello, I.; Lifshitz, Y. *Science* **2000,** 287, (5450), 104-106.

32. McDonough, J. K.; Frolov, A. I.; Presser, V.; Niu, J.; Miller, C. H.; Ubieto, T.; Fedorov, M. V.; Gogotsi, Y. *Carbon* **2012,** 50, (9), 3298-3309.

33. Hahm, M. G.; Leela Mohana Reddy, A.; Cole, D. P.; Rivera, M.; Vento, J. A.; Nam, J.; Jung, H. Y.; Kim, Y. L.; Narayanan, N. T.; Hashim, D. P.; Galande, C.; Jung, Y. J.; Bundy, M.; Karna, S.; Ajayan, P. M.; Vajtai, R. *Nano Lett.* **2012,** 12, (11), 5616-5621.

34. Bom, D.; Andrews, R.; Jacques, D.; Anthony, J.; Chen, B.; Meier, M. S.; Selegue, J. P. *Nano Lett.* **2002,** 2, (6), 615-619.

35. Morelos-Gómez, A.; Vega-Díaz, S. M.; González, V. J.; Tristán-López, F.; Cruz-Silva, R.; Fujisawa, K.; Muramatsu, H.; Hayashi, T.; Mi, X.; Shi, Y.; Sakamoto, H.; Khoerunnisa, F.; Kaneko, K.; Sumpter, B. G.; Kim, Y. A.; Meunier, V.; Endo, M.; Muñoz-Sandoval, E.; Terrones, M. *ACS Nano* **2012,** 6, (3), 2261-2272.

36. Li, W.; Liang, C.; Zhou, W.; Qiu, J.; Zhou; Sun, G.; Xin, Q. *J. Phys. Chem. B* **2003,** 107, (26), 6292-6299.

37. Wang, Y.; Yu, S. F.; Sun, C. Y.; Zhu, T. J.; Yang, H. Y. *J. Mater. Chem.* **2012,** 22, (34), 17584-17588.

38. Zhao, M.-Q.; Zhang, Q.; Huang, J.-Q.; Tian, G.-L.; Chen, T.-C.; Qian, W.-Z.; Wei, F. *Carbon* **2013,** 54, (0), 403-411.

39. Pech, D.; Brunet, M.; Durou, H.; Huang, P.; Mochalin, V.; Gogotsi, Y.; Taberna, P.-L.; Simon, P. *Nature Nanotech.* **2010,** 5, (9), 651-654.

40. Wang, H.; Wang, Y.; Hu, Z.; Wang, X. *ACS Appl. Mater. Interfaces* **2012,** 4, (12), 6827-6834.

41. Tsai, W.-Y.; Gao, P.-C.; Daffos, B.; Taberna, P.-L.; Perez, C. R.; Gogotsi, Y.; Favier, F.; Simon, P. *Electrochem. Commun.* **2013,** 34, (0), 109-112.

42. An, K. H.; Kim, W. S.; Park, Y. S.; Moon, J. M.; Bae, D. J.; Lim, S. C.; Lee, Y. S.; Lee, Y. H. *Adv. Funct. Mater.* **2001,** 11, (5), 387-392.

43. Sevilla, M.; Fuertes, A. B. *ACS Nano* **2014,** 8, (5), 5069-5078.

44. Wang, H.; Xu, Z.; Kohandehghan, A.; Li, Z.; Cui, K.; Tan, X.; Stephenson, T. J.; King'ondu, C. K.; Holt, C. M. B.; Olsen, B. C.; Tak, J. K.; Harfield, D.; Anyia, A. O.; Mitlin, D. *ACS Nano* **2013,** 7, (6), 5131-5141.

45. Yan, J.; Wang, Q.; Wei, T.; Jiang, L.; Zhang, M.; Jing, X.; Fan, Z. *ACS Nano* **2014,** 8, (5), 4720-4729.

46. Wu, Z.-S.; Wang, D.-W.; Ren, W.; Zhao, J.; Zhou, G.; Li, F.; Cheng, H.-M. *Adv. Funct. Mater.* **2010,** 20, (20), 3595-3602.

47. Cheng, Y.; Lu, S.; Zhang, H.; Varanasi, C. V.; Liu, J. *Nano Lett.* **2012,** 12, (8), 4206-4211.

48. Kaempgen, M.; Chan, C. K.; Ma, J.; Cui, Y.; Gruner, G. *Nano Lett.* **2009,** 9, (5), 1872-1876.

49. Fan, Z.; Yan, J.; Wei, T.; Zhi, L.; Ning, G.; Li, T.; Wei, F. *Adv. Funct. Mater.* **2011,** 21, (12), 2366-2375.

50. Chen, Z.; Augustyn, V.; Wen, J.; Zhang, Y.; Shen, M.; Dunn, B.; Lu, Y. *Adv. Mater.* **2011,** 23, (6), 791-795.

51. Choi, B. G.; Yang, M.; Hong, W. H.; Choi, J. W.; Huh, Y. S. *ACS Nano* **2012,** 6, (5), 4020-4028.

52. Kim, T.; Jung, G.; Yoo, S.; Suh, K. S.; Ruoff, R. S. *ACS Nano* **2013,** 7, (8), 6899-6905.

Table of Contents Graphic
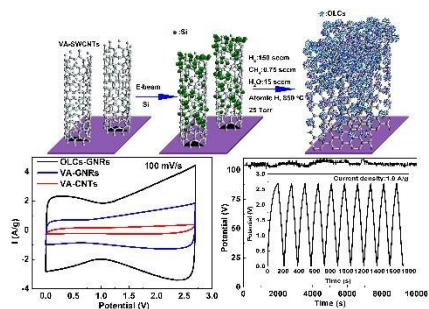
Carbon composite materials consisting of OLCs and VA-GNRs which preserved of vertical structural integrity and alignment have been realized by atomic hydrogen treatment.